J Sol-Gel Sci Technol (2017) 81:413–422
DOI 10.1007/s10971-016-4216-8

ORIGINAL PAPER: FUNDAMENTALS OF SOL-GEL AND HYBRID MATERIALS PROCESSING

Study on structure and fluorescence of Tb-doped CaAl LDHs prepared in ethanol/water system

Yufeng Chen[1] · Xiaoqing Wang[1] · Yao Bao[1] · Weinan Wu[1]

Received: 9 May 2016 / Accepted: 20 September 2016 / Published online: 1 October 2016

Abstract An important material applied in biological fluorescent detector and medical treatment is highly desired in view of the biocompatibility and fluorescent property. Here, Tb-doped CaAl-layered double hydroxides with $Ca^{2+}/(Al^{3+} + Tb^{3+})$ molar ratio of 1.0, 2.0, 3.0, and 4.0 have been successfully prepared in a mixed solution of ethanol and water in a reasonable proportion. Chemical compositional analyses revealed that the experimental value of $Ca^{2+}/(Al^{3+} + Tb^{3+})$ molar ratio present in the samples was close to the initial value of $Ca^{2+}/(Al^{3+} + Tb^{3+})$ molar ratio of raw reactants. In the *X-ray diffraction* results, it was found that the typical layered double hydroxides structure can be kept between the $Ca^{2+}/(Al^{3+}+Tb^{3+})$ molar ratio of 1.0 and 4.0. The structural type of the Tb-doped CaAl-layered double hydroxides was monoclinic form when the Tb content was less than of 3.0 %, while rhombohedral form appeared and retained as the content of Tb^{3+} is kept between 3.0 and 5.28 wt%. Photoluminescence shows strong green emissions attributed to $^5D_4$-^7F_J ($J = 3$, 4, 5, 6) transition of Tb^{3+} ions incorporated in the Tb-doped CaAl-layered double hydroxides.

Graphical Abstract A series of Tb-doped CaAl-LDHs with different molar ratio of $Ca^{2+}/(Al^{3+} + Tb^{3+})$ have been synthesized by co-precipitation in a mixed ethanol/water system. Strong green emission appeared in the Tb-doped CaAl-LDH. The Tb–CaAl-LDHs may be a promising biological fluorescent material because of the biocompatibility of Ca^{2+} ions as well as the fluorescent property of Tb^{3+} ions.

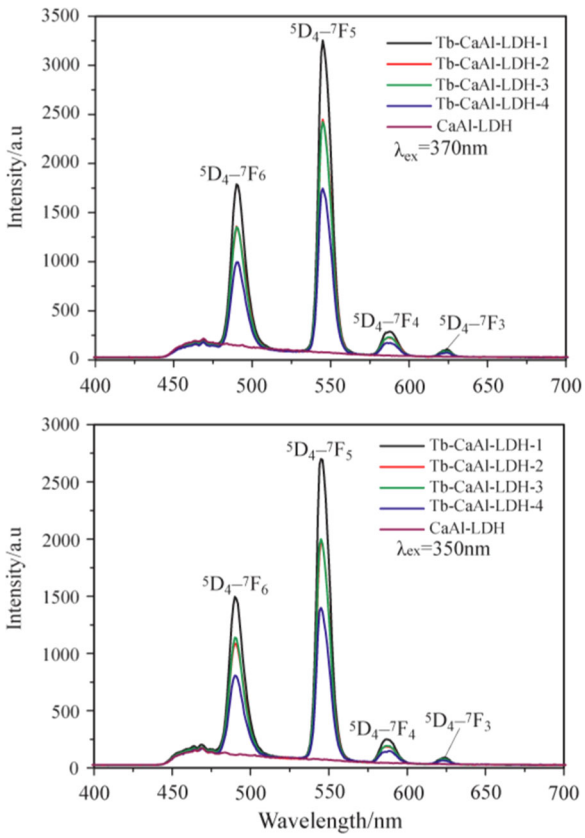

✉ Yufeng Chen
yfchen@ncu.edu.cn

[1] College of Chemistry, Nanchang University, Nanchang 330031, China

Keywords CaAl-LDH · Tb dopant · Fluorescence

1 Introduction

Layered double hydroxides (LDH) have been extensively studied because of their potential application in adsorbents, catalysts or catalyst supports, supercapacitors, biological, and pharmaceutical materials, etc [1–5]. An interesting group of LDHs named as hydrocalumite has chemical formula of $Ca_2Al(OH)_6Cl{\cdot}2H_2O$ or $Ca_4Al_2O_6Cl_2{\cdot}10H_2O$ [PDF#19-0202, PDF#31-0245, PDF#44-0615, PDF# 54-0852, PDF# 35-0105, 6, 7], and a net positive charge on the sheets originates from the partial replacement of Ca^{2+} with Al^{3+} ions, forming $[Ca_2Al(OH)_6]^+$ layer. The hydrocalumites attracted far less attention because of the relative difficulty in synthesizing pure forms of the material by common methods. Consequently, more studies focused on its synthesis and the exploitations of its properties and potential applications. Therefore, various methods have been developed, such as co-precipitation method [8], microwave irradiation or synthesis [9, 10], reconstruction method [11], hydrothermal crystallization technique [12], surfactant directed synthesis [13], and multi-step processes [14], etc. However, the Ca–Al LDHs with various anions have been used as adsorbing materials [7, 15–21], concrete hardening accelerators [22–24], treatment of landfill leachate [25], catalysts or catalyst supports [26–30], and flame retardant [31–33], etc.

In addition, trivalent terbium ion is an important dopant producing green emissions, and the development of stable and inexpensive Tb-doped fluorescent materials for biotechnological applications has been a central problem in modern materials science. Although there are many studies on Tb-doped inorganic materials [34–37] or Tb-complexes [38–40], these Tb-doped inorganic materials are often related to high temperature energy consumption [41, 42], and Tb-complexes have poor thermal stability. For this reason, it is important to prepare the Tb-doped inorganic materials at room temperatures.

In consideration of the biocompatibility of Ca^{2+}ions [43, 44] and green emission of Tb^{3+} ions, Tb-doped CaAl-LDH would be more potential application in biological techniques and medical treatment compared with other LDHs. For instance, CaAl-LDH may be an important material in drug packaging, drug transport, and drug storage and release, etc. For this purpose, Tb^{3+} ions were incorporated into layers of CaAl-LDHs by co-precipitation in a mixed solution of ethanol and water with reasonable proportion, and different structural types of Tb-doped CaAl-LDHs with fluorescent property have been obtained. This special interlayer tuning structure of Tb–CaAl-LDHs may be a promising biological fluorescent material because of the biocompatibility of Ca^{2+} ions as well as the fluorescent property of Tb^{3+} ions.

2 Experimental

2.1 Synthesis of materials

CaAl-LDH and Tb–CaAl-LDH-*n* ($n = 1$, 2, 3, 4) were prepared by an ethanol/water solution route [22]. A batch of solution with $Ca^{2+}/(Al^{3+}+Tb^{3+})$ molar ratio of 1.0, 2.0, 3.0, and 4.0 was separately prepared by dissolving $CaCl_2$ and $AlCl_3{\cdot}6H_2O$ solid in ultrapure water and mixed with Tb $(NO_3)_3$ solution (each of 100 mL, labeled as A). $Tb(NO_3)_3$ solution was prepared by dissolving Tb_2O_3 solid in mixed solution of concentrated nitric acid and hydrogen peroxide solution. NaOH ($1.0\ mol{\cdot}L^{-1}$) solution was prepared from ultrapure water and analytical grade solid NaOH. Four of mixed media with ethanol/water volume ratio of 2/3 was obtained (each of 200 mL, labeled as B), and kept its temperature at 50 °C.

Then each of solution A (100 mL) and $1.0\ mol{\cdot}L^{-1}$NaOH solution were simultaneously added dropwise into each of the 200 mL solution B at 50 °C and severely stirred. Then a series of slurry formed at pH values of 10.5~11.5. The resulting slurry was aged in reacting system (50 °C) for 4 h. After being filtrated, washed, and dried at 70 °C, Tb-doped CaAl-LDHs with different $Ca^{2+}/(Al^{3+}+Tb^{3+})$ molar ratios have been obtained. The samples corresponding to initial Ca/(Al + Tb) molar ratio of 1.0, 2.0, 3.0, 4.0 were signed as Tb–CaAl-LDH-1, Tb–CaAl-LDH-2, Tb–CaAl-LDH-3, and Tb–CaAl-LDH-4, respectively. The CaAl-LDH with Ca/Al molar ratio of 2.0 was prepared by the same method as above.

2.2 Characterization

Chemical contents of Ca, Al, Tb, and O were measured by inductively coupled plasma atomic emission spectroscopy (ICP-AES Optima 5300DV) and scanning electron microscopy equipped with chemical analyses (SEM/EDX, JEOL JSM-6701). The content of Cl element was estimated by gas chromatography-mass spectrometry (GC-MS Agilent-6890N/59731) and SEM/EDX. The H content was determined basing on CHN elemental analysis (Elementar Vario EL II, Germany) and thermogravimetric analysis. Under nitrogen atmosphere at a scan rate of 10 °C/min, thermogravimetric results were obtained using synchronous thermal analyzer (Pyris Diamovd, American Pe Company). The chemical formulas were estimated basing on the results of ICP, GC-MS, TG-DTA, SEM-EDX, and CHN elemental analyses as well as the principle of charge balance. Powder X-ray diffraction patterns were collected using a Shimadzu

Table 1 Chemical composition of CaAl-LDH and Tb–CaAl-LDH-*n* ($n = 1, 2, 3, 4$)

Samples	Ca/(Al + Tb) molar ratio		Tb content %	Mass loss % (temperature range)
	Initial	Experimental		
CaAl-LDH	2.0	1.98	0 %	22.4 % (30~316 °C)
	Chemical formula	$Ca_{1.98}Al(OH)_{5.96}Cl{\cdot}3.9H_2O$		
Tb–CaAl-LDH-1	1.0	1.08	5.28 %	22.4 % (30~330 °C)
	Chemical formula	$Ca_{1.08}Al_{0.92}Tb_{0.08}(OH)_{4.16}Cl{\cdot}3.0H_2O$		
Tb–CaAl-LDH-2	2.0	1.96	3.32 %	25.2 % (30~319 °C)
	Chemical formula	$Ca_{1.96}Al_{0.93}Tb_{0.07}(OH)_{5.92}Cl{\cdot}4.7H_2O$		
Tb–CaAl-LDH-3	3.0	2.95	3.0 %	23.4 % (30~319 °C)
	Chemical formula	$Ca_{2.95}Al_{0.92}Tb_{0.08}(OH)_{7.90}Cl{\cdot}5.5H_2O$		
Tb–CaAl-LDH-4	4.0	3.97	2.34 %	26.2 % (30~308 °C)
	Chemical formula	$Ca_{3.97}Al_{0.92}Tb_{0.08}(OH)_{9.94}Cl{\cdot}7.9H_2O$		

Chemical formula estimations based on the results of ICP, EDX, CHN elemental analysis, and mass loss

model XD3A diffractometer with Cu K_a radiation ($\lambda = 1.54$ Å, 40 kV e, 30 mA), a scan range from $2\theta = 3$ to 60° and at a scan rate of 2°/min. Infrared spectra were recorded on a Shimadzu IR spectrometer (Prestige-21) in the range of 4000–400 cm^{-1} The fluorescent property of the samples was investigated with the help of F-7000 FL Spectrophotometer.

3 Results and discussion

3.1 Composition and structurue analyses

The chemical compositions of CaAl-LDH and Tb–CaAl-LDH-*n* ($n = 1, 2, 3, 4$) were determined based on the ICP, SEM-EDX, CHN elemental analysis, and thermogravimetric analysis (seen in Table 1 and Fig. 1). Ca, Al, Cl, and O signals appeared in the EDX spectra of all the samples (seen in Fig. 1), and no Tb signal exhibited in the EDX spectrum of the CaAl-LDH. Moreover, the Tb signal is very weak because of small Tb content and the insensitivity of Tb element to the measurement of EDX. In addition, C signal occurring in the EDX spectra of all the samples was may be due to physically adsorbed CO_2. In view of the compositional analyses (shown in Table 1), the experimental values of $Ca^{2+}/(Al^{3+} + Tb^{3+})$ molar ratios present in the samples were close to the initial $Ca^{2+}/(Al^{3+} + Tb^{3+})$ molar ratios of raw reactants. A matter worthy of note is that the Tb content of the Tb–CaAl-LDH-*n* ($n = 1, 2, 3, 4$) gradually decreased with the increasing *n* value, which is in accordance with the initial reactants.

Figure 2 displays the XRD patterns of the CaAl-LDH and Tb–CaAl-LDH-*n* ($n = 1, 2, 3, 4$). The XRD pattern of the CaAl-LDH was in excellent agreement with that recorded on PDF 31-0245 in the database of the International Center for Diffraction Data, with a nominal chemical formula of $Ca_4Al_2O_6Cl_2{\cdot}\ 10H_2O$. Based on the XRD data of the CaAl-LDH and the literature [PDF 31-0245], all the reflections were indexed as in Fig. 2. The cell parameters of the CaAl-LDH could be refined as $a = 9.763(7)$ Å, $b = 5.700(4)$ Å, $c = 16.97(2)$ Å, $\beta = 113.07(7)°$, which were in accordance with the values ($a = 9.853$ Å, $b = 5.715$ Å, $c = 16.898$ Å, $\beta = 113.33°$) [PDF 31-0245]. The structural type belongs to monoclinic form. In addition, the CaAl-LDH presents diffraction peaks corresponding to (002), (004), (020), and (006) crystal planes, indicating relatively well-formed crystalline layered structure, with the basal spacing d_{002} of 7.7 Å. This interlayer spacing is similar to those of literatures [14, 22]. The crystallinity of the CaAl-LDH is better than those of other CaAl-Cl LDHs [14, 15], and analogous to that of the literature [22].

While small content of Tb^{3+} (2.34 %wt) was doped into the CaAl-LDH (seen Tb–CaAl-LDH-4), the structural type did not change, but the cell parameters varied as $a = 9.75(2)$ Å, $b = 5.717(8)$ Å, $c = 16.81(4)$ Å, $\beta = 112.9(2)°$, which may be due to the effect of Tb^{3+} doping. With the content of Tb^{3+} up to 3.0 %wt (shown in the Tb–CaAl-LDH-3), the reflection (021) disappeared, and the structural type changed from monoclinic to rhombohedral form. Although the content of Tb^{3+} was further increased to 5.28 wt%, the rhombohedral form still remained the same. All the reflections matched well with that recorded on PDF 35-0105 in the database of the International Center for Diffraction Data, with a nominal chemical formula of $Ca_2Al(OH)_6Cl{\cdot}2H_2O$, corresponding cell parameters of $a = 5.742$ Å, $b = 5.742$ Å, $c = 46.847$ Å, and $\beta = 120°$. These results indicated that the structural type of CaAl-LDHs could be transformed by doping a certain content of Tb^{3+}. It was worthwhile to note that most of the CaAl-LDHs were focused on the LDH with the Ca^{2+}/Al^{3+} molar of 2 except for very few studies related to the initial Ca^{2+}/Al^{3+} molar

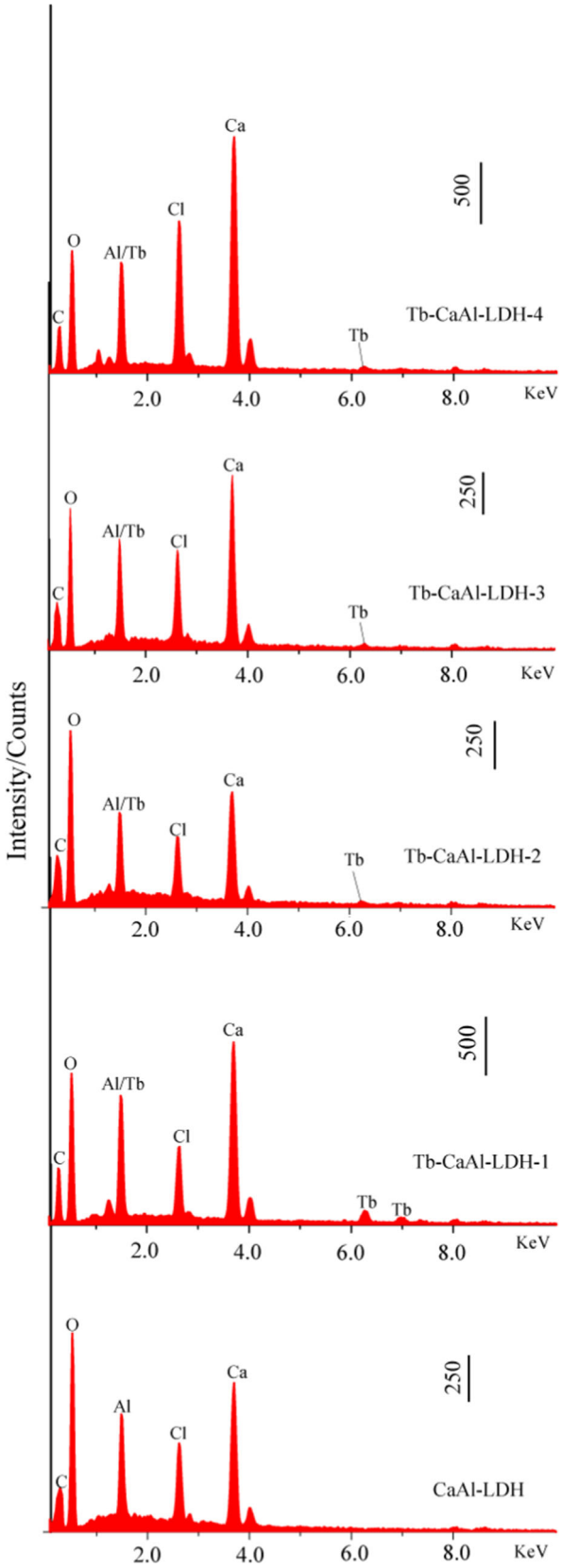

Fig. 1 EDX Results of CaAl-LDH, Tb–CaAl-LDH-1,Tb–CaAl-LDH-2, Tb–CaAl-LDH-3, and Tb–CaAl-LDH-4

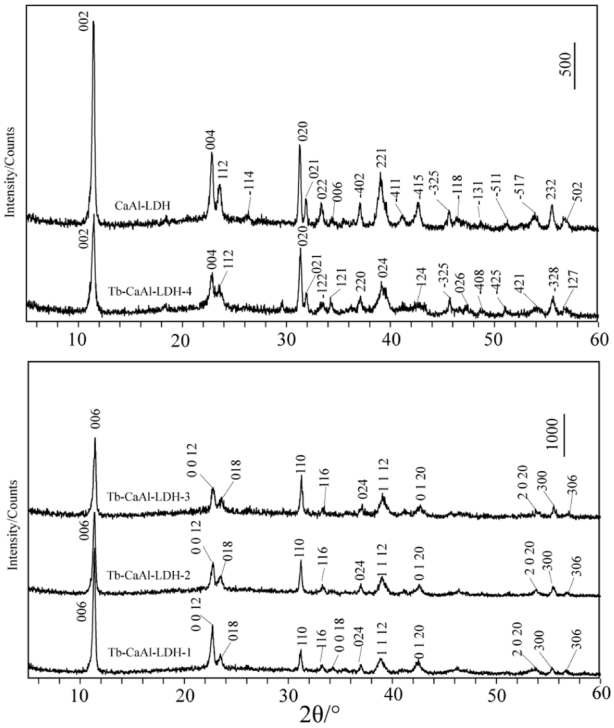

Fig. 2 XRD patterns of CaAl-LDH, Tb–CaAl-LDH-1,Tb–CaAl-LDH-2, Tb–CaAl-LDH-3, and Tb–CaAl-LDH-4

ration of 1–6 [45]. However, the present compositional results revealed that the LDH structure can be kept between the $Ca^{2+}/(Al^{3+} + Tb^{3+})$ molar ratio of 1.0 and 4.0. In addition, the *scanning electron microscope* (SEM) images (seen in Fig. 3) did not obviously change although the structural type transformed. The SEM images of LDHs are different from that of the previous report [12], but similar to the literature [45], which may be due to different preparation processes or conditions.

3.2 FT-IR spectra

The IR spectra of CaAl-LDH and Tb–CaAl-LDH-*n* ($n = 1$, 2, 3, 4) in 4000–400 cm^{-1} are shown in Fig. 4. For the CaAl-LDH, characteristic bands appeared in 3640 and 3485 cm^{-1}, attributed to the stretching vibrations of lattice water and OH groups, respectively, and the band at 1623 cm^{-1} is owing to the bending mode of O–H [15]. The bands at 793 and 591 cm^{-1} are due to stretching vibration of M–OH and M–O–M. It is well known that IR spectroscopy is very sensitive to CO_2 or carbonate anions in LDHs. The presence of the physisorbed CO_2 is reflected by the relative broad peak at 1409 cm^{-1} typical of O–C–O vibrations (ν_3) for adsorbed (non interlayer) carbonate anions that are present on the outer surface of the crystallites [26, 46]. After the Tb^{3+} ions were incorporated into the layers of CaAl-LDH, all the bands present in the IR spectra did not

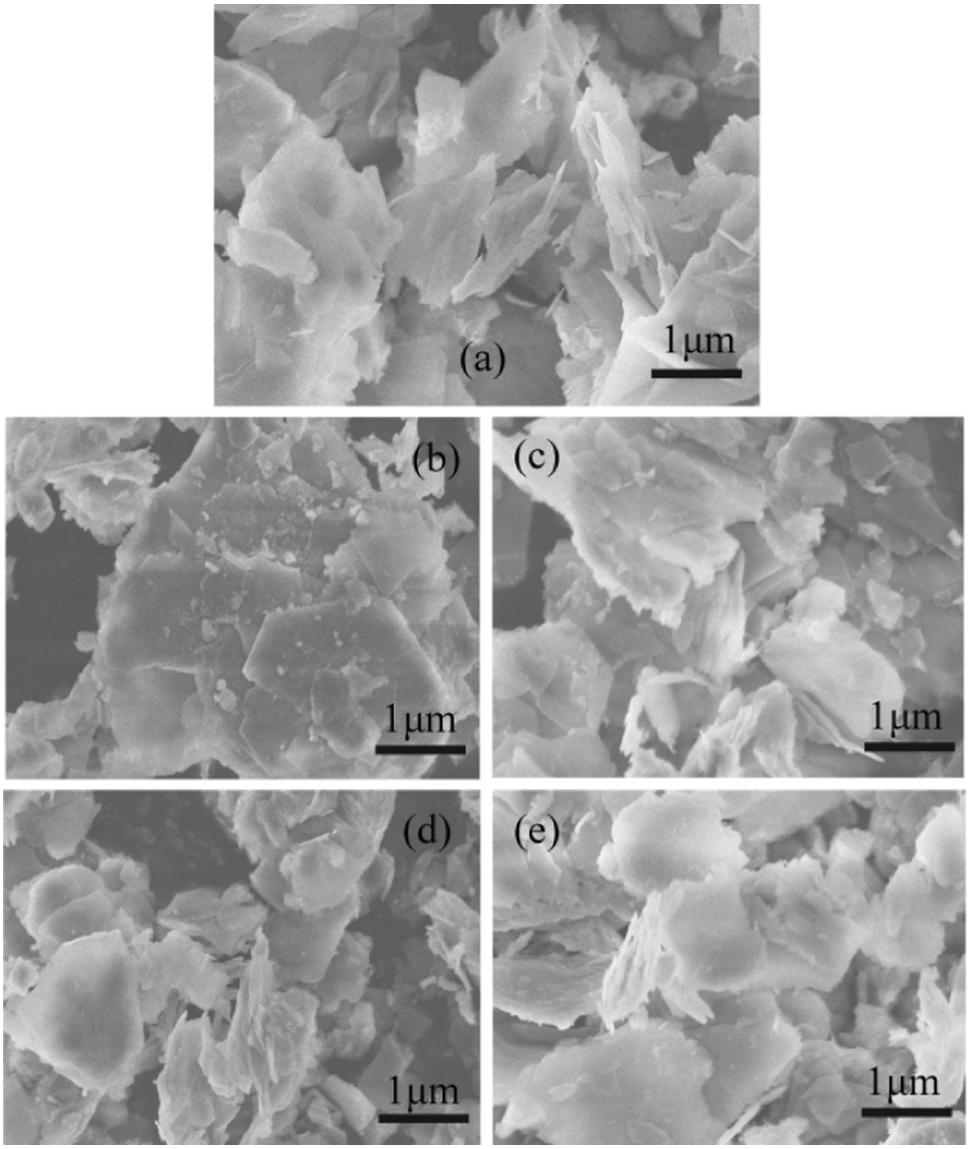

Fig. 3 SEM images of. **a** CaAl-LDH, **b** Tb–CaAl-LDH-1, **c** Tb–CaAl-LDH-2, **d** Tb–CaAl-LDH-3, and **e** Tb–CaAl-LDH-4

obviously shift, suggesting the layered structure of LDH retained. In addition, the band at 1409 cm^{-1} attributed to physisorbed CO_2 obviously increased with the increase in the content of Tb^{3+}, which may be due to highly positive charge of Tb^{3+} more easily adsorbed CO_2.

3.3 Thermogravimetric analyses

TGA-DTG-DTA curves of CaAl-LDH and Tb–CaAl-LDH-*n* ($n = 1, 2, 3, 4$) represented in Fig. 5. The decomposing stages of all samples have been presented in Table 2. According to TGA and DTG curves, the decomposition of CaAl-LDH exhibited three stages. The first one occurred in 30–114 °C, corresponding to the loss of the adsorbed water and some of bound water [45]; the second stage in 114–316 °C was mainly due to the loss of interlayer water of the hydrocalumite [45, 47]; and the third stage was attributed to the further removal of hydroxyl groups and Cl^- [45]. This thermal decomposition was similar to that of Ca_2Al LDH [45]. After Tb^{3+} was incorporated into the layers of CaAl-LDH, the Tb–CaAl-LDH-1, Tb–CaAl-LDH-2, and Tb–CaAl-LDH-3 had similar TGA-DTG-DTA curves as that of the CaAl-LDH, it also exhibited three stages of decomposition (seen in Table 2) corresponding to the loss of the adsorbed water and bound water, interlayer water, and hydroxyl of layers and Cl^-, respectively. In contrast, the thermal decomposition of Tb–CaAl-LDH-4 was very different, and four mass loss stages appeared in 30–54, 54–124, 124–308, and 308–688 °C, which is due to the loss of physically adsorbed water, bound water, interlayer water, and hydroxyl of layers and Cl^-, respectively. The different thermal decomposition of the Tb–CaAl-LDH-4 from that of

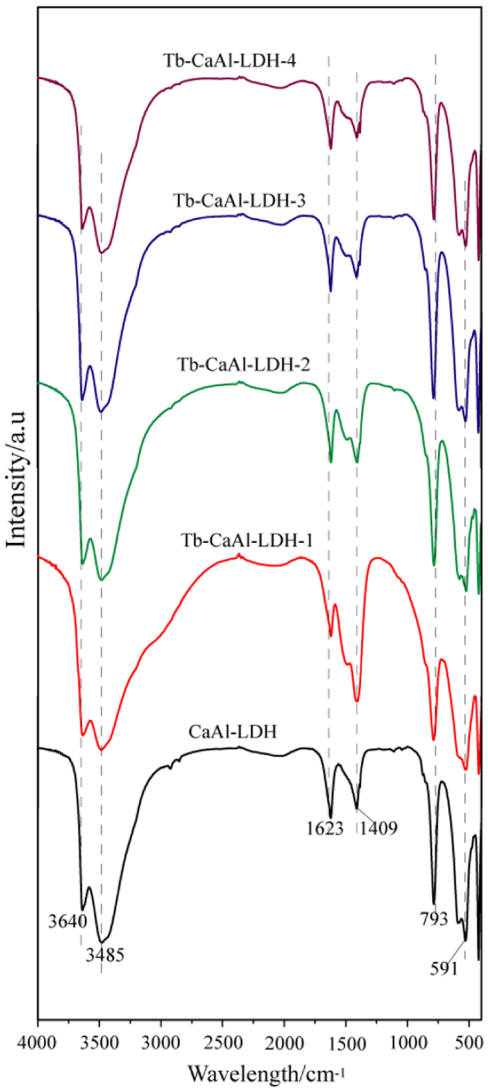

Fig. 4 FT-IR spectra of CaAl-LDH, Tb–CaAl-LDH-1,Tb–CaAl-LDH-2, Tb–CaAl-LDH-3, and Tb–CaAl-LDH-4

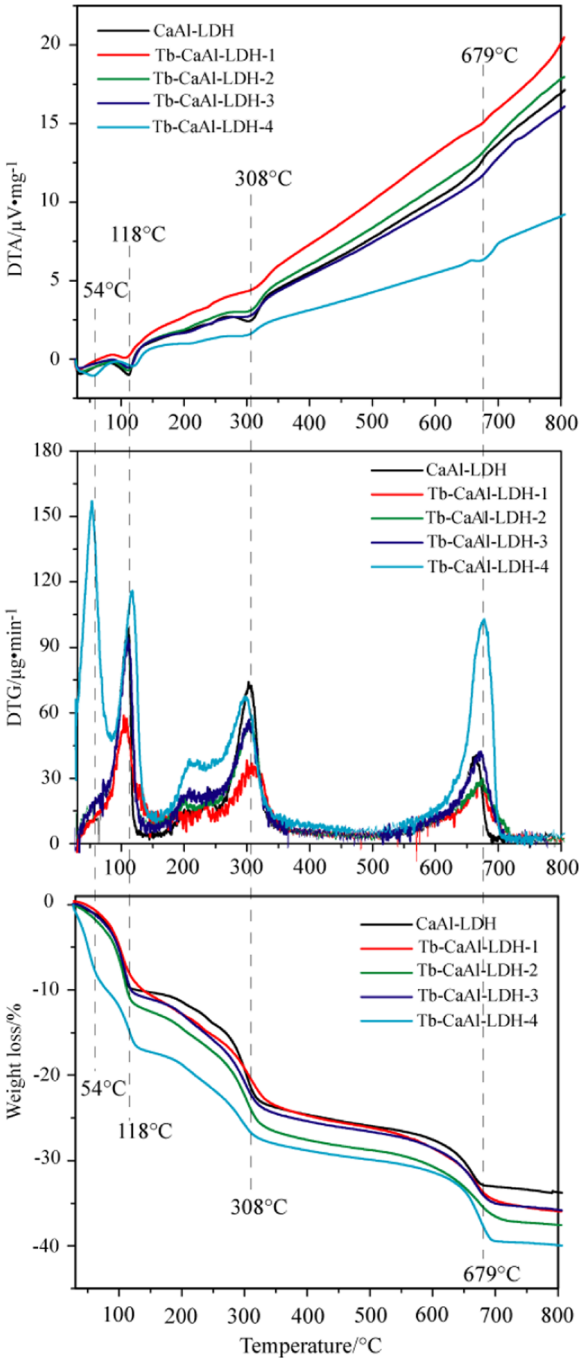

Fig. 5 TG-DTA-DTG curves of CaAl-LDH, Tb–CaAl-LDH-1, Tb–CaAl-LDH-2, Tb–CaAl- LDH-3, and Tb–CaAl-LDH-4

the CaAl-LDH, Tb–CaAl-LDH-1, Tb–CaAl-LDH-2, and Tb–CaAl-LDH-3 may be due to different content of water present in the samples. Meanwhile, two endothermic peaks appeared in the DTA curves of the CaAl-LDH, Tb–CaAl-LDH-1, Tb–CaAl-LDH-2, and Tb–CaAl-LDH-3, which may be due to the evaporation of physically adsorbed water and bound water as well as the interlayer water. Four endothermic peaks occurred in the DTA curve of the Tb–CaAl-LDH-4, attributed to the evaporation of the physically adsorbed water, bound water, interlayer water, and hydroxyl of layers, respectively. It was worthwhile to notice that although the Tb–CaAl-LDH-4 has similar crystal structure with CaAl-LDH and other Tb–CaAl-LDH-n (n = 1, 2, 3) according to their XRD patterns, its TGA-DTA curves are very different from other samples. The possible reasons are that the TGA-DTA curves of LDHs are often subjected to various factors, including chemical composition, structure, crystallinity, and interlayer water and anions, etc. In consideration to the present XRD patterns, chemical composition, and interlayer guests of the samples, the difference between the TG-DTA curves of the Tb–CaAl-LDH-4 and those of other samples may be are mainly due to the different content of interlayer water. Meanwhile the TG-DTA curves of the Tb–CaAl-LDH-4 are below than that of

Table 2 Thermogravimetric results of CaAl-LDH and Tb–CaAl-LDH-*n* ($n = 1, 2, 3, 4$)

Samples	Stage1	Stage2	Stage3	Stage4
CaAl-LDH	30~114 °C/9.6 %	117~316 °C/12.8 %	316~675 °C/10.3 %	
Tb–CaAl-LDH-1	30~118 °C/8.4 %	118~330 °C/14.0 %	330~678 °C/11.2 %	
Tb–CaAl-LDH-2	30~114 °C/10.7 %	114~319 °C/14.5 %	319~688 °C/10.7 %	
Tb–CaAl-LDH-3	30~118 °C/10.0 %	118~319 °C/13.4 %	319~688 °C/11.2 %	
Tb–CaAl-LDH-4	30~54 °C/6.3 %	54~124 °C/10.1 %	124~308 °C/10.2 %	308~688 °C/12.8 %

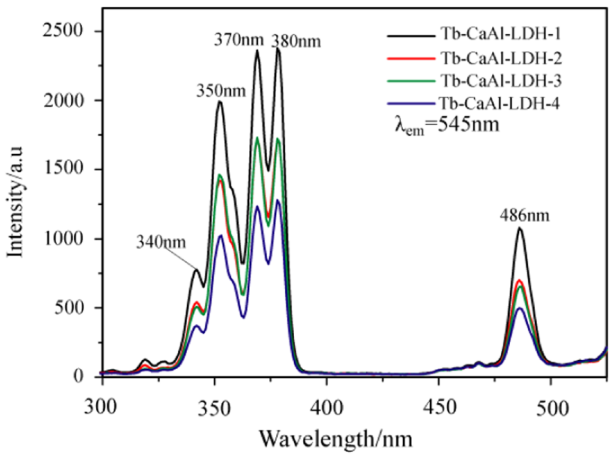

Fig. 6 Excitation spectra of CaAl-LDH, Tb–CaAl-LDH-1,Tb–CaAl-LDH-2, Tb–CaAl-LDH-3, and Tb–CaAl-LDH-4

other samples, indicating poorer thermal stability of the Tb–CaAl-LDH-4 compared with those of other four samples.

3.4 Fluorescent analyses

Figure 6 shows excitation spectra of CaAl-Tb–LDH-*n* ($n = 1, 2, 3, 4$). The excitation spectra were obtained at an emission wavelength of 545 nm, which corresponds to the $^5D_4 \rightarrow {}^7F_5$ transition emission of Tb^{3+}(III). The strong excitation bands due to $^7F_6 \rightarrow {}^5G_4$, $^7F_6 \rightarrow {}^5L_{10}$, and $^7F_6 \rightarrow {}^5G_6$ electronic transitions appeared at 350, 370, and 380 nm, respectively [48, 49]. A weak excitation band emerged at 340 nm may be owing to $^7F_6 \rightarrow {}^5D_2$ [50]. Compared with the Tb–CaAl-LDHs, no obvious excitation bands occurred in the CaAl-LDH at the emission wavelength of 545 nm. In the light of the excitation spectra of samples, emission spectra recorded at room temperature for all the samples were obtained in the optimum excitation wavelength of 350 and 370 nm (shown in Fig. 7). The emission spectra of Tb–CaAl-LDH-*n*($n = 1, 2, 3, 4$) show two strong green emissions at 545 and 490 nm attributed to $^5D_4 \rightarrow {}^7F_5$ and $^5D_4 \rightarrow {}^7F_6$ transition of Tb^{3+}, respectively [51–54]. The peaks due to $^5D_4 \rightarrow {}^7F_3$ and $^5D_4 \rightarrow {}^7F_4$ transition are very weak. With regard to the CaAl-LDH, no peaks attributed to

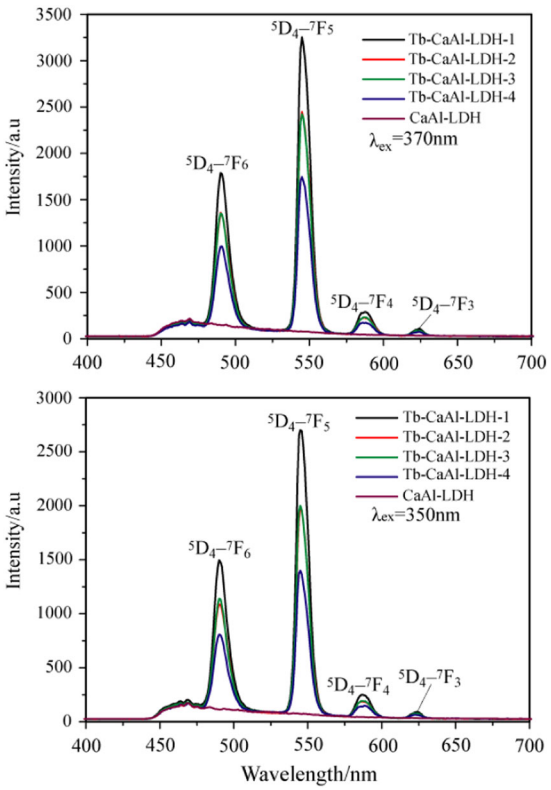

Fig. 7 Emission spectra of CaAl-LDH, Tb–CaAl-LDH-1,Tb–CaAl-LDH-2, Tb–CaAl-LDH-3, and Tb–CaAl-LDH-4 with excitation wavelength of 350 and370 nm, respectively

$^5D_4 \rightarrow {}^7F_J$ ($J = 3, 4, 5, 6$) transition appeared. It is worthwhile to noting that the green emissions attributed to $^5D_4 \rightarrow {}^7F_5$ and $^5D_4 \rightarrow {}^7F_6$ transition of Tb^{3+} incorporated in CaAl-LDHs have similar intensity as those of organic Tb-complexes [55–59], and are even stronger than those of other Tb-doped MgAl-LDH and Tb-doped ZnAl-LDH [60–62]. The excellent fluorescent property of Tb-doped CaAl-LDH makes it be a promising biological fluorescent material because of the biocompatibility of Ca^{2+}.

Figure 8 displays the ratio of the ($^5D_4 \rightarrow {}^7F_5$)/($^5D_4 \rightarrow {}^7F_6$) emission intensity (namely asymmetric parameter *R*) depending on the molar ratios of $Ca^{2+}/(Al^{3+} + Tb^{3+})$. Because the $^5D_4 \rightarrow {}^7F_5$ transition of Tb^{3+} is highly hypersensitive to Tb^{3+} surroundings and the $^5D_4 \rightarrow {}^7F_6$ transition

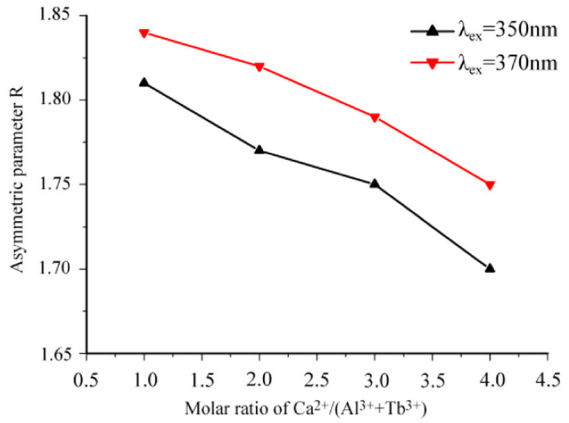

Fig. 8 Asymmetric parameter R as function of molar ratios of $Ca^{2+}/(Al^{3+}+Tb^{3+})$

is independent of its environment, the *R* value can give some valuable information about the symmetry of the site in which Tb^{3+} ions are situated [63]. It was found that the ratio of the $(^5D_4\rightarrow{}^7F_5)/(^5D_4\rightarrow{}^7F_6)$ emission intensity obviously decreased with the increase in the molar ratio of $Ca^{2+}/(Al^{3+} + Tb^{3+})$, suggesting the different surroundings of Tb^{3+}. The highest ratio presents in the sample with $Ca^{2+}/(Al^{3+} + Tb^{3+})$ molar ratio of 1.0, revealing distorted local environment of the Tb^{3+} ion; the lowest ratio in the sample with $Ca^{2+}/(Al^{3+} + Tb^{3+})$ molar ratio of 4.0, corresponding to lower distorted local environment of the Tb^{3+} ion. The decrease in the ratio of the $(^5D_4\rightarrow{}^7F_5)/(^5D_4\rightarrow{}^7F_6)$ emission intensity with the increasing molar ratio of $Ca^{2+}/(Al^{3+}+Tb^{3+})$ indicated the less lattice distortion in the local environment of the Tb^{3+} ion due to fewer divalent metal ions (Ca^{2+}) isomorphously substituted by trivalent metal ions ($Al^{3+} + Tb^{3+}$) in the LDH framework. This result was in accordance with the previous work [62].

4 Conclusion

We have synthesized a series of Tb-doped CaAl-LDHs with fluorescent property in a mixed solution of ethanol and water with reasonable proportion. Various techniques, including ICP, CHN, SEM-EDX, XRD, IR, TGA-DTA-DTG, and FL, were used to characterize the chemical composition, structure, and fluorescent property of samples. Results indicated that all the Tb-doped samples present typical structure of LDH and strong green emissions attributed to $^5D_4\rightarrow{}^7F_5$ transition of Tb^{3+} ions. Moreover, the content of Tb^{3+} incorporated in the CaAl-LDHs affected the structural type of CaAl-LDHs. In addition, the content of interlayer water of Tb–CaAl-LDH-*n*($n = 1, 2, 3, 4$) has influence on their thermal stability. In the light of the biocompatibility of Ca^{2+} and excellent green emission of Tb^{3+}, the Tb-doped CaAl-LDHs will be potential application in biological fluorescent materials.

Acknowledgments The Project was supported by the National Natural Science Foundation of China (Grant No.51162021).

Compliance with ethical standards

Conflict of interest The authors declare that they have no competing interests.

References

1. Li T, Li GH, Li LH, L iu L, Xu Y, Ding HY, Zhang T (2016) Large-scale self-assembly of 3D flower-like hierarchical Ni/Co-LDHs microspheres for high-performance flexible asymmetric supercapacitors. ACS Appl Mater Inter 8:2562–2572
2. Xu SM, Pan T, Dou YB, Yan H, Zhang ST, Ning FY, Shi WY, Wei M (2015) Theoretical and experimental study on $M^{II}M^{III}$-layered double hydroxides as efficient photocatalysts toward oxygen evolution from water. J Phys Chem C 119:18823–18834
3. Chen YF, Zhou SH, Li F, Chen YW (2010) Synthesis and photoluminescence of Eu-doped Zn/Al layered double hydroxides. J Mater Sci 45:6417–6423
4. Zargoosh K, Kondori S, Dinari M, Mallakpour S (2015) Synthesis of layered double hydroxides containing a biodegradable amino acid derivative and their application for effective removal of cyanide from industrial wastes. Ind Eng Chem Res 54:1093–1102
5. Wang J, Zhu RR, Gao B, Wu B, Li K, Sun XY, Liu H, Wang SL (2014) The enhanced immune response of hepatitis B virus DNA vaccine using SiO2@LDH nanoparticles as an adjuvant. Biomater 35:466–478
6. Vieille L, Taviot-Guého C, Besse JP, Leroux F (2003) Hydrocalumite and its polymer derivatives. 2. polymer incorporation versus in situ polymerization of styrene-4-sulfonate. Chem Mater 15:4369–4376
7. Sá FP, Cunha BN, Nunes LM (2013) Effect of pH on the adsorption of sunset yellow FCF food dye into a layered double hydroxide (CaAl-LDH-NO_3). Chem Eng J 215–216:122–127
8. Rojas R (2014) Copper, lead and cadmium removal by Ca Al layered double hydroxides. Appl Clay Sci 87:254–259
9. Pérez-Barrado E, Pujol MC, Aguiló M, Cesteros Y, Díaz F, Pallarès J, Marsal FL, Salagre P (2013) Fast aging treatment for the synthesis of Ca–Al–Cl LDHs using microwaves. Appl Clay Sci 80/81:313–319
10. Szabados M, Mészáros R, Erdei S, Kónya Z, KukoveczÁ., Sipos P, Pálinkó I (2016) Ultrasonically-enhanced mechanochemical synthesis of CaAl-layered double hydroxides intercalated by a variety of inorganic anions. Ultrasonics Sonochem 31:409–416
11. Pérez-Barrado E, Salagre P, Marsal LF, Aguiló M, Cesteros Y, Díaz F, Pallarès J, Cucinotta F, Marchese L, Pujol MC (2015) Ultrasound-assisted reconstruction and delamination studies on CaAl layered double hydroxidesm. Appl Clay Sci 118:116–123
12. Dutta K, Pramanik A (2013) Synthesis of a novel cone-shaped CaAl-layered double hydroxide (LDH): its potential use as a reversible oil sorbent. Chem Commun 49:6427–6429
13. kawee AW, Sch€aeffel F, Warner JH, O'Hare D (2012) Surfactant directed synthesis of calcium aluminum layered double hydroxides nanoplatelets. J Mater Chem 22:7751–7756
14. Zhang P, Qian GR, Xu ZP, Shi HS, Ruan XX, Yang J, Frost RL (2012) Effective adsorption of sodium dodecylsulfate (SDS) by hydrocalumite (CaAl-LDH-Cl) induced by self-dissolution and re-precipitation mechanism. J Collo Interf Sci 367:264–271

15. Zhang P, Qian GR, Cheng HF, Yang J, Shi HS, Frost RL (2011) Near-infrared and mid-infrared investigations of Na-dodecylbenzenesulfate intercalated into hydrocalumite chloride (CaAl-LDH-Cl). Spectrochimica Acta Part A 79:548–553
16. Liu XJ, Ge L, Li W, Wang XZ, Li F (2015) Layered double hydroxide functionalized textile for effective oil/water separation and selective oil adsorption. ACS Appl Mater Interf 7:791–800
17. Li YL, Wang J, Li ZS, Liu Q, Liu JY, Liu LH, Zhang XF, Yu J (2013) Ultrasound assisted synthesis of Ca–Al hydrotalcite for U (VI) and Cr (VI) adsorption. Chem Eng J 218:295–302
18. Xu YF, Dai YC, Zhou JZ, Xu ZP, Qian GR, Lu GQM (2010) Removal efficiency of arsenate and phosphate from aqueous solution using layered double hydroxide materials: intercalation vs. precipitation. J Mater Chem 20:4684–4691
19. Qian G, Feng L, Zhou JZ, Xu Y, Liu J, Zhang J, Xu ZP (2012) Solubility product (ksp)-controlled removal of chromate and phosphate by Ca–Al–Cl LDH. Chem Eng J 181/182:251–258
20. Li SN, Bai HB, Wang J, Jing XY, Liu Q, Zhang ML, Chen RR, Liu LH (2012) In situ grown of nano-hydroxyapatite on magnetic CaAl-layered double hydroxides and its application in uranium removal. Chem Eng J 193/194:372–380
21. Qiu X, Sasaki K, Yu T, Hirajima T, Ideta K, Jin M (2015) Mechanism of boron uptake by Ca–Al–Cl LDH calcined at different temperatures. J Hazard Mater 287:268–277
22. Xu SL, Zhang BW, Chen ZR, Yu JH, Evans DG, Zhang FZ (2011) A General and scalable formulation of pure CaAl-layered double hydroxide via an organic/water solution route. Ind Eng Chem Res 50:6567–6572
23. Xu SL, Chen ZR, Zhang BW, Yu JH, Zhang FZ, Evans DG (2009) Facile preparation of pure CaAl-layered double hydroxides and their application as a hardening accelerator in concrete. Chem Eng J 155:881–885
24. Chen YX, Shui ZH, Chen W, Chen GW (2015) Chloride binding of synthetic Ca–Al–NO3 LDHs in hardened cement Paste. Construct Buil Mater 93:1051–1058
25. Chen H, Sun Y, Ruan XX, Yu Y, Zhu MY, Zhang J, Zhou JZ, Xu YF, Liu JY, Qian GR (2016) Advanced treatment of stabilized landfill leachate after biochemical process with hydro-calumite chloride (Ca/Al–Cl LDH). Biores Technol. doi:10.1016/j.biortech.2016.01.035
26. Campos-Molina MJ, Santamarí a-Gonz_alez J, Mérida-Robles J, Moreno-Tost R, Albuquerque MCG, Bruque-Gámez S, Rodríguez-Castellón E, Jiménez-López A, Maireles-Torres P (2010) Base catalysts derived from hydrocalumite for the transesterification of sunflower oil. Energy Fuels 24:979–984
27. Buffet JC, Wanna N, Arnold TAQ, Gibson EK, Wells PP, Wang Q, Tantirungrotechai J, O'Hare D (2015) Highly tunable catalyst supports for single-site ethylene polymer-rization. Chem Mater 27:1495–1501
28. Feng JT, He YF, Liu YN, Du YY, Li DQ (2015) Supported catalysts based on layered double hydroxides for catalytic oxidation and hydrogenation: general functionality and promising application prospects. Chem Soc Rev 44:5291–5319
29. Pérez-Barrado E, Pujol MC, Aguiló M, Llorca J, Cesteros Y, Díaz F, Pallarès J, Marsal LF, Salagre P (2015) Influence of acid–base properties of calcined MgAl and CaAl layered double hydroxides on the catalytic glycerol etherification to short-chain Polyglycerols. Chem. Eng. J. 264:547–556
30. Cota I, Ramírez E, Medina F, Sueiras JE, Layrac G, Tichit D (2010) New synthesis route of Ca–Al–Cl LDH-Type materials and their application as basic catalysts for aldol condensation. Appl Clay Sci 50:498–502
31. Gao YS, Wu JW, Wang Q, Wilkieb CA, O'Hare D (2014) Flame retardant polymer/layered double hydroxide nanocomposites. J Mater Chem A 2:10996–11016
32. Matusinovic Z, Lu HD, Wilkie CA (2012) The role of dispersion of LDH in fire retardancy: The effect of dispersion on fire retardant properties of polystyrene/CaAl layered double hydroxide Nanocomposites. Polym Degrad Stab 97:1563–1568
33. Matusinovic Z, Feng JX, Wilkie CA (2013) The role of dispersion of LDH in fire retardancy: The effect of different divalent metals in benzoic acid modified LDH on dispersion and fire retardant properties of polystyrene- and poly(methyl-methacrylate)-LDH-B nanocomposites. Polym Degrad Stab 98:1515–1525
34. Han J, Wang L, Wong SS (2014) Observation of Photoinduced Charge Transfer in Novel Luminescent CdSe Quantum Dot–$CePO_4$:Tb Metal Oxide Nanowire Composite Heterostructures. J Phys Chem C 118:5671–5682
35. Puchalska M, Zych E, Sobczyk M, Watras A, Deren P (2015) Cooperative energy transfer in Yb^{3+}-Tb^{3+} co-doped $CaAl_4O_7$ upconverting phosphor. Mater Chem Phys 156(2015):220–226
36. Guo QF, Liao LB, Mei LF, Liu HK, Hai Y (2015) Color-tunable photoluminescence phosphors of Ce^{3+} and Tb^{3+} co-doped $Sr_2La_8(SiO_4)_6O_2$ for UV w-LEDs. J Solid State Chem 225:149–154
37. Ayvackl M, Canimoglu A, Karabulut Y, Kotan Z, Herval LKS, Godoy MPF, GalvoGobato Y, Henini M, Can N (2014) Radioluminescence and photoluminescence characterization Of Eu andTb doped barium stannate phosphor ceramics. J Alloys Compds 590:417–423
38. Yue B, Chen YN, Chu HB, Qu YR, Wang AL, Zhao YL (2014) Synthesis, crystal structures and fluorescence properties of dinuclear Tb(III) and Sm(III) complexes with, 4,6-tri(2-pyridyl)-1,3,5-triazine and halogenated benzoic acid. Inorg Chimica Acta 414:39–45
39 Greig NE, Einkauf JD, Clark JM, Corcoran EJ, Karrama JP, Kent CA, Eugene VE, Chan BC, Lill DT (2015) Luminescent lanthanide coordination polymers synthesized via in-situ hydrolysis of dimethyl-3,4-furandicarboxylate. J Solid State Chem 225:402–409
40 Gao BJ, Qiao ZW, Chen T (2014) Structure and photoluminescence property of complexes of aromatic carboxylic acid-functionalized polysulfone with Eu(III) and Tb(III). Mater Chem Phys 143:1119–1130
41. Soares JV, Gugliotti CF, Kawashima YS, Tatumi SH, Mittani JCR (2014) Thermo- luminescence and optically stimulated luminescence characteristics of Al_2O_3 doped with Tb. Radia Measurements 5:15–20
42. Kawashima YS, Gugliotti CF, Yee M, Tatumi SH, Mittani JCR (2014) Thermoluminescence features of MgB_4O_7:Tb phosphor. Radia Phys Chem 95:91–93
43. Sánchez-Salcedo S, Colilla M, Izquierdo-Barba I, Vallet-Reg M (2013) Design and preparation of biocompatible zwitterionic hydroxyapatite. J Mater Chem B 1:1595–1606
44. Ding YF, Wen C, Hodgson P, Li YC (2014) Effects of alloying elements on the corrosion behavior and biocompatibility of biodegradable magnesium alloys: a review. J Mater Chem B 2:1912–1933
45. Zheng LP, Xia SX, Lu XY, Hou ZY (2015) Ransesterification of glycerol with dimethyl carbonate over calcined Ca-Al hydrocalumite. Chin J Catal 36:1759–1765
46. Qu J, Zhong LH, Li Z, Chen M, Zhang QW, Liu XZ (2016) Effect of anion addition on the syntheses of Ca–Al layered double hydroxide via a two-step mechanochemical process. Appl Clay Sci. doi:10.1016/j.clay.2016.02.026
47. Zhang J, Xu YF, Qian GR, Xu ZP, Chen C, Liu Q (2010) Reinvestigation of Dehydration and Dehydroxylation of Hydrotalcite-like Compounds through Combined TG-DTA-MS Analyses. J Phys Chem C 114:10768–10774
48. Sohn Y (2014) Structural and spectroscopic characteristics of terbiumhydroxide/oxide Nanorods and plates. Ceram Intert 40:13803–13811

49. Jyothy PV, Amrutha KA, Gijo J, Unnikrishnan NV (2009) Fluorescence enhancement in Tb^{3+}/CdS nanoparticles doped silica xerogels. J Fluoresc 19:165–168
50. Davesnne C, Ziani A, Labbé C, Marie P, Frilay C, Portier X (2014) Energy transfer mechanism between terbium and europium ions in zinc oxide and zinc silicates thin films. Thin Solid Films 553:33–37
51. Feng LJ, Tian Y, Wang L, Cui C, Shi QF, Huang P (2016) Tunable emission, energy transfer, and thermal stability of Ce^{3+}-doped and Ce^{3+}/Tb^{3+} Co-doped $Ca_9Sr(PO_4)_6C_{12}$ phosphors. J Mater Sci 51:2841–2849
52. Zhu ZZ, Fu GS, Yang Y, Yang ZP, Li PL (2016) Energy transfer, tunable luminescence, and thermal stability of Tb^{3+}–Sm^{3+}-codoped $Na_3Bi(PO_4)_2$ phosphors. J Mater Sci 51:6944–6954
53. Zhu XZ, Chu CL, Chu PK (2016) Synthesis and cathodoluminescent properties of Lu_3(Al,Ga)5O12:Tb^{3+} with and without niobium-doped TiO2coating. J Sol-Gel Sci Technol 77:355–360
54. Fadeyev E, Smola S, Snurnikova O, Korovin O, Rusakova N (2013) Luminescent sol–gel materials based on lanthanide aminopolycarboxylates (Ln=Nd, Eu, Tb, Yb). J Sol-Gel Sci Technol 68:479–487
55. Stan CS, Marcotte N, Secula MS, Popa M (2014) A new photoluminescent silica aerogel based On N-hydroxysuccinimide–Tb (III) complex. J Sol-Gel Sci Technol 69:207–213
56. Lin JT, Zheng YH, Wang. QM (2015) Conversion of Lewis acid-base interaction into readable emission outputs by novel terbium hybrid nanosphere. Dyes and Pigments 112:239–244
57. Spencer EC, Zhao J, Ross NL, Andrews MB, Surbella RG, Cahill CL (2013) The influence of pressure on the photoluminescence properties of aterbium-adipate framework. J Solid State Chem 202:99–104
58. Khorasani-Motlagh M, Noroozifar M, Niroom S, Moodi A (2013) Photoluminescence studies of aTerbium(III) complex as a fluorescent probe for DNA detection. J Lumin 143:56–62
59. Hildebrandt N, Wegner KD, Algar WR (2014) Luminescent terbium complexes: Superior Förster resonance energy transfer donors for flexible and sensitive multiplexed biosensing. Coord Chem Rev 273/274:125–138
60. Chen YF, BaoY YuZP, Yang GC, Wang XQ (2016) Photoluminescence of Tb-doped MgAl-LDHs depending on phase transition caused by annealing Photoluminescence of Tb-doped MgAl-LDHs depending on phase transition caused by annealing. J Rare Earths 34:39–45
61. Chen YF, Bao Y, Wang XQ (2016) Green Emission of Tb-doped Mg-Al Layered Double Hydroxide Response to L-lysine. J Fluores 26:813–820
62. Chen YF, Bao Y, Yang GC, Yu ZP (2016) Study on structure and photoluminescence of Tb-doped ZnAl-NO_3 layered double hydroxides prepared by co-precipitation Study on structure and photoluminescence of Tb-doped ZnAl-NO_3 layered double hydroxides prepared by co-precipitation. Mater Chem Phys 176:24–31
63. Marques APA, Motta V, Cruz MA, AVarela J, Longo E, Rosa IL V (2011) $BaMoO_4$:Tb^{3+} phosphor properties: synthesis, characterization and photophysical studies. Solid State Ion 202:54–59